

STABILITY CHARACTERISTICS OF CROSSFLOW MODES IN HYPERSONIC BOUNDARY LAYER WITH EXPANSION CORNER

Peisen Lu¹, Youcheng Xi¹, Jiamiao Sun¹ & Song Fu¹

¹Tsinghua University, Beijing, China

Abstract

The expansion corner is a common feature on the wings of hypersonic vehicles with a significant impact on crossflow instabilities. This study aims to investigate how the expansion corner affects instabilities under real three-dimensional hypersonic flow conditions. We focus on hypersonic swept flows over a wing model designed to mimic actual vehicles. The flow is calculated at a free-stream Mach number of 6 with an adiabatic wall condition. The model consists of a blunt cone, followed by an expansion corner and a flat plate. Laminar flow computations with different swept angles are conducted using in-house shock-fitting procedures to ensure the accuracy of the base flow. We employ linear stability theory (LST) and secondary instability theory (SIT) to understand how the expansion corner influences crossflow instabilities. Both growth rates curves and neutral curves are calculated to illuminate the instabilities in this regime. Our results show that the expansion corner has a destabilizing effect on the crossflow modes in this case.

Keywords: Hypersonic, Expansion, Stability, Crossflow

1. General Introduction

1.1 Research Background

In the realm of aerodynamic studies, the instability and transition phenomenon of the boundary layer holds a prominent position as a typical flow phenomenon on aircraft surfaces. This phenomenon can lead to a significant increase in skin friction and heat flux, making it closely related to the design of the vehicle's thermal protection system. However, due to the strong nonlinearity and sensitivity of the flow itself, the transition of hypersonic flows still presents numerous challenges[1].

The three-dimensional boundary layer on the actual vehicle surface is subject to various instability mechanisms that can trigger transition, such as attachment line instability, streamwise instability, centrifugal Görtler instability, and crossflow instability, with crossflow stability being particularly important. Unlike two-dimensional boundary layers, the typical feature of three-dimensional boundary layers is that inviscid instabilities may dominate over traditional viscous instabilities, such as Tollmien-Schlichting (T-S) waves, as the primary instability mechanism[2]. Within this context, Hall[3] pointed out that the significance of centrifugal Görtler instability diminishes substantially when the sweep angle surpasses a certain threshold relative to the Reynolds number raised to the power of one-half (Re-1/2). Consequently, the dominant instability mechanisms become either T-S instability or crossflow instability.

Crossflow, a secondary flow in the three-dimensional boundary layer, is induced by an imbalance between the pressure gradient perpendicular to the potential flow direction and the centripetal force. This secondary flow has a velocity profile with an inflection point, making it primarily governed by the inviscid instability mechanisms defined in traditional stability analysis. Typical models for studying crossflow include swept wings, corner flows, swirling disks, and blunted cones with an angle of attack. The stability characteristics of the three-dimensional boundary layer are often investigated using modal analysis methods. Crossflow modes can be classified into two overarching categories: stationary waves characterized by zero frequency, and traveling waves characterized by specific frequencies[4].

The most unstable traveling wave mode typically has a frequency much lower than that of the T-S mode and the second Mack mode. Stationary wave disturbances are commonly attributed to wall roughness-induced excitations, whereas traveling wave disturbances primarily arise due to the turbulence intensity within the freestream flow. Deyhle[5] pointed out that, despite the generally higher growth rates predicted by linear stability theory for traveling wave modes, empirical evidence suggests that in instances of low turbulence intensity in the incoming flow, the transition is often instigated by stationary wave modes. Therefore, studying the stability characteristics of steady crossflow modes can help understand the physical factors influencing transition under actual flight conditions.

The phenomenon of crossflow instability transition was first observed by Gray[6] in 1952 during the flight tests of the AW52 at the Royal Aircraft Establishment in the UK. In these tests, the swept wing experienced transition earlier than the unswept wing, with sublimation lines of kaolin observed before transition, aligned with the direction of inviscid potential flow, somewhat similar to the two-dimensional Görtler vortex transition. The study speculated that stationary streamwise vortices were generated within the boundary layer. Owen and Randell, Squire, Stuart[7][8][9] conducted theoretical and experimental studies on this phenomenon in 1952, primarily by defining the crossflow Reynolds number to investigate the conditions under which crossflow transition occurs, finding the critical crossflow Reynolds number to be approximately 150. The goal of these studies was to achieve full laminar flow on swept wing surfaces to enhance aerodynamic efficiency.

Early theoretical analyses of crossflow stability mainly focused on incompressible rotating disk flows because this type of crossflow is very similar to that on swept wings, and the basic flow of rotating disk provides similarity solutions, facilitating early research analyses. Another practical model for studying crossflow is the Falkner-Skan-Cooke boundary layer, which allows control of crossflow intensity through β_h and θ . Smith[10] first observed the characteristics of crossflow vortices on rotating disk surfaces in 1946, noting that they formed an angle of 90+14° with the radius. Gregory et al.[11] in 1955 derived the three-dimensional stability equations for rotating disk flows and conducted experimental studies on both rotating disks and swept wings, discussing the concepts of stationary and traveling waves and indicating that the primary instability mechanism was inflectional instability caused by crossflow velocity. Brown solved the disturbance equations directly, obtaining results consistent with those of Gray and Owen on the AW52 configuration in 1959[12], and he provided a critical Reynolds number of about 180 for incompressible rotating disk flows in 1961[13]. Cebeci and Stewartson[14] obtained critical parameters similar to Brown's for rotating disk flows and produced neutral stability curves in 1980. Wilkinson and Malik[15], in their experiments on incompressible rotating disk flows in 1983, first discovered that stationary vortices were initiated from randomly distributed point sources on the disk, and they artificially added roughness elements, observing secondary instability disturbances in the late transition stage. They reported a critical Reynolds number of about 280, significantly different from Brown's[13] and Cebeci's[14] results (around 170), mainly because earlier theories did not consider the effect of curvature. Malik's[16] theoretical analysis yielded a critical Reynolds number of 287, while Kobayashi's[17] result was 261, closely matching the experimental values. These theoretical analyses indicated that traveling wave disturbances have higher growth rates than stationary disturbances[18]. Furthermore, Malik[19] computed the neutral stability curves for stationary disturbances in more detail in 1986, finding a critical Reynolds number of 285.36 and discovering a second minimum on the lower branch of the neutral curve, corresponding to an angle of 19.5°, explaining the anomalous crossflow vortex angles observed by Fedorov[20]. The upper branch matched Stuart's[11] asymptotic solution, while the lower branch corresponded to disturbances in the direction of zero wall shear, with Fedorov's experiments showing subcritical instabilities near this lower branch. Faller[21] provided neutral stability curves and critical Reynolds numbers for various conditions in incompressible rotating disk flows in 1991, consistent with Malik's results for stationary[19] and traveling[22] disturbances. Further studies on incompressible rotating disk flows can be seen in Hall[23] and Morkovin[24].

Early theoretical and experimental achievements were mainly applied to the design of laminar wings for low-speed and transonic airfoils, using control methods like blowing and suction. Pfenninger et al.[25][26][27] conducted a series of experiments on 30-degree swept wings, validating Brown's results with blowing and suction and successfully achieving full laminar flow on the X-21 wing. Mack[28]

studied the effect of compressibility on crossflow instability in 1979, finding that compressibility reduced the growth rate and altered the direction of the instability waves. El-Hady[29] and Mack[30] analyzed crossflow instability for the 23° supercritical swept wing configuration at NASA Langley Center, showing the impact of suction distribution on crossflow mode growth rates. Nayfeh and Padhye[31][32][33], using complex group velocity, further developed Gaster's[34] classic time mode and spatial mode conversion relationship for three-dimensional boundary layers, deriving disturbance equations considering non-parallel effects under incompressible and compressible conditions through multi-scale methods. Their analysis of the X-21 wing revealed that non-parallelism made crossflow modes more unstable.

With advancements in theoretical and experimental capabilities, the study of crossflow traveling wave disturbances and their interactions with stationary disturbances, the nonlinear evolution of crossflow disturbances, and secondary instabilities has been furthered. DLR's Bippes[35][36][37], ASU's Saric [38][39][40], and ONERA's Arnal[41], among others, have conducted experiments on the linear and nonlinear growth of crossflow vortices. ASU and ONERA focused on low-speed experiments on infinite-span swept wing models, while DLR applied additional pressure gradients above swept wings through a specific setup. The Nonlinear Parabolized Stability Equations (NPSE) method was successfully applied to study the nonlinear evolution of stationary crossflow vortices. Malik et al.[42] studied secondary instability of stationary crossflow vortices on low-speed swept wings in 1999, showing that the transition location predicted by secondary instability (N-factor) correlated better with experimental results than those predicted by primary instability methods. Haynes et al.[43] compared linear and nonlinear stability analysis tools for low-speed swept wings with ASU's experimental results, showing that both Linear Stability Theory (LST) and NPSE could accurately capture the linear growth and nonlinear saturation of stationary crossflow vortices.

Further secondary instability analysis tools, such as the Floquet theory-based Secondary Instability Theory (SIT), Bi-Global stability analysis, and Direct Numerical Simulation (DNS), have also been widely applied in crossflow stability analysis[44][45][46][42][47][48]. Balachandar et al.[49] performed secondary instability analysis on rotating disk flows, discovering high-frequency secondary instability disturbances similar to those in Kohama's[50] experiments. Fisher and Dallmann[51] used secondary instability theory in 1991, while Meyer and Kleiser in 1988[52] used DNS to theoretically analyze Müller and Bippes' experiments[35]. Fisher and Dallmann suggested that the traveling wave disturbances observed in experiments were secondary instabilities of stationary crossflow vortices rather than primary instability characteristics of three-dimensional boundary layers. Meyer and Kleiser observed saturation of two modes in their DNS, consistent with experimental results. Malik et al. in 1996 classified secondary instability modes into Type I and Type II. Type I modes are primarily induced by spanwise gradients of the streamwise velocity in the basic flow, while Type II modes are primarily induced by normal gradients of the streamwise velocity in the basic flow.

Interest in hypersonic research has also been increasing. Experimentally studying high-speed crossflow transition is challenging, mainly conducted using impulse wind tunnels. FLDI can be used to study Mack mode disturbances[54], but it cannot measure small-scale crossflow structures. Hot-wire anemometry can only measure data at one location and for a very short duration [55]. Currently, experimental data are mostly limited to surface pressure, temperature, and heat flux. The largest hypersonic crossflow-related flight experiments to date are part of the HiFIRE program[56][57]. Its research models include a cone (HiFIRE-1) and an ellipsoid cone (HiFIRE-5). However, these models also lack boundary layer measurement data. Additionally, these models are used to approximate hypersonic glider shapes, experiencing both crossflow instability and Mack mode instability. In 2016, Craig and Saric[4] measured traveling crossflow modes and Type I modes, though higher-frequency modes were not captured. In 2015, Ward, Henderson, and Schneider[58] measured second modes and Type II modes. Kocian's [59] review detailed experimental and computational results for this model at an incoming Mach number of around 6. These experiments are usually conducted in quiet tunnels, with numerical studies primarily using NPSE and Bi-Global methods, and experimental and theoretical results corroborating each other well. The findings indicate that, aside from the new streamwise instability mode (Mack's second mode) appearing under hypersonic conditions, crossflow instability exhibits many similarities with low-speed conditions. However, under hypersonic conditions, sec-

ondary instability of crossflow vortices shows saturation[4], and the frequency of secondary instability modes can be very close to Mack's second mode under certain conditions, potentially leading to mode interactions[60]. Other significant hypersonic models include the HyTRV model from the China Aerodynamics Research and Development Center, which isolates the effects of various instability mechanisms by dividing the geometry into several main regions[61]. More recent results on hypersonic crossflow stability analysis can be found in [62][63][64][65][66].

Although there have been studies on hypersonic crossflow stability for various geometries such as flat plates and blunt cones, research on crossflow stability for complex models remains limited and insufficient. This study aims to utilize a linear stability framework to analyze the impact of typical expansion corner structures on the growth rate of the steady crossflow mode in a three-dimensional boundary layer, which further provides a theoretical basis for the analysis of the transition mechanism influenced by expansion corners on hypersonic vehicles.

1.2 Problem Statement

The focal point of investigation pertains to a meticulously designed wing model representative of actual vehicles. This model comprises a blunt cone with half-angle of 6 degrees followed by an expansion corner and a flat plate. The aerodynamic calculations are conducted at a free-stream Mach number of 6, under adiabatic wall conditions. The sweep angle ranges from zero to 60 degrees, and the present discourse exclusively presents outcomes pertaining to the 60-degree sweep angle configuration. The model follows the ideal gas assumption of air. The calculation parameters are listed in Table 1.

Table 1 – Calculation parameters for the swept wing

Re	T_{∞}	R	Pr	γ
3.521×10^6	224K	2mm	0.72	1.4

2. Methodology

2.1 Baseflow Calculation

Hypersonic stability analysis requires high-quality laminar baseflow calculation. To obtain a smooth and accurate fundamental flow field, this paper employs a high-order accurate shock-fitted finite difference method for the calculation of the swept baseflow.

Since this method uses moving shocks as the far-field boundary, the program adopts a dynamic grid method, and there exists the following transform relationship between the physical coordinates and the computational coordinates:

$$\begin{cases}
\xi = \xi(x, y, t) \\
\eta = \eta(x, y, t) \\
\zeta = z \\
\tau = t
\end{cases}, J = \begin{vmatrix}
x_{\xi} & x_{\eta} & 0 & x_{\tau} \\
y_{\xi} & y_{\eta} & 0 & y_{\tau} \\
0 & 0 & 1 & 0 \\
0 & 0 & 0 & 1
\end{vmatrix}.$$
(1)

The control equation is the Navier-Stokes equation for compressible fluids, which is expressed as follows:

$$\frac{1}{J}\frac{\partial U}{\partial \tau} + \frac{\partial F_{inv}}{\partial \xi} + \frac{\partial G_{inv}}{\partial \eta} + \frac{\partial H_{inv}}{\partial \zeta} + U\frac{\partial}{\partial \tau}\left(\frac{1}{J}\right) = \frac{1}{\text{Re}}\left[\frac{\partial F_{vis}}{\partial \xi} + \frac{\partial G_{vis}}{\partial \eta} + \frac{\partial H_{vis}}{\partial \zeta}\right].$$
 (2)

The expressions for the conservative variables, viscous flux and inviscid flux are:

$$U = \begin{bmatrix} \rho \\ \rho u \\ \rho v \\ \rho w \\ \rho E \end{bmatrix}$$

$$F_{inv} = \frac{F\xi_x + G\xi_y + H\xi_z}{J}, F = \begin{bmatrix} \rho u \\ \rho u^2 + p \\ \rho uv \\ \rho uw \\ (E+p)u \end{bmatrix}$$
(3)

Besides, the working fluid is air, satisfying the assumptions of the ideal gas. The viscosity is calculated by Sutherland's law. The baseflow is calculated using in-house shock-fitting DNS code[67]. The fifth-order upwind scheme (for inviscid flux) of Zhong[68] together with the sixth-order centre scheme (for viscous flux) is used to compute the flow field. Here, the Rankine-Hugoniot relation is satisfied at the shock boundary. A fourth-order Runge—Kutta method is applied for the time integration. By treating the shock wave as a sharp interface, high accuracy can be achieved in the whole flow field, which is an essential prerequisite for the stability analysis.

2.2 Linear Stablility Theory (LST)

The LNS equations are derived from the NS equations by introducing small perturbations, subtracting the basic flow equations and ignoring the nonlinear terms. A frequently employed form is commonly written as

$$\Gamma \frac{\partial \Phi}{\partial t} + \mathbf{A} \frac{\partial \Phi}{\partial x} + \mathbf{B} \frac{\partial \Phi}{\partial y} + \mathbf{C} \frac{\partial \Phi}{\partial z} + \mathbf{D} \Phi = \mathbf{H}_{xx} \frac{\partial^2 \Phi}{\partial x^2} + \mathbf{H}_{xy} \frac{\partial^2 \Phi}{\partial x \partial y} + \mathbf{H}_{xz} \frac{\partial^2 \Phi}{\partial x \partial z} + \mathbf{H}_{yy} \frac{\partial^2 \Phi}{\partial y^2} + \mathbf{H}_{yz} \frac{\partial^2 \Phi}{\partial y \partial z} + \mathbf{H}_{zz} \frac{\partial^2 \Phi}{\partial z^2}.$$
(4)

For local analysis, the perturbations can be written in a wave-like form as

$$\Phi(x, y, z, t) = \phi(y) \exp(i\alpha x + i\beta z - i\omega t) + \text{c.c.}$$
 (5)

As only stationary waves are investigated, omega is assumed to be zero. The generalized eigenvalue problem of LST presents

$$\mathcal{L}_l \phi = \alpha \mathcal{R}_l \phi \tag{6}$$

2.3 Grid Generation Algorithm

The computational grid is a curvilinear body-fitted structured code-generated grid. The meshing strategy ensures a smooth transition in the distribution of grid spacing in the flow direction, and the spacing is densified near the leading edge and the expansion corner. The streamwise grid spacing is determined by

$$F = \sum_{i=1}^{4} a_{i} \operatorname{erf} \left[\sigma_{i} \left(\xi - b_{i} \right) + (-1)^{e_{i}} \right]$$

$$x = x(\xi), \frac{d^{2}x}{d\xi^{2}} = \frac{F}{2\Delta_{s}} \frac{dx}{d\xi},$$

$$x(0) = 0, x(1) = 1, \xi \in [0, 1].$$
(7)

In the wall-normal direction, grids cluster near the wall surface in the following manner:

$$y = a \frac{1+\eta}{b-\eta}, a = \frac{y_i y_{\text{max}}}{y_{\text{max}} - 2y_i}, b = 1 + \frac{2a}{y_{\text{max}}}, \eta \in [-1, 1].$$
 (8)

The distribution of the spacing in the streamwise direction and the overall glance of the grid is shown in Fig.1. After testing the grid independence, the final grid number is 1001×201. The three-dimensional sketch of the swept wing model is shown in Fig.2, and the cyan part of the figure represents the surface of the swept wing.

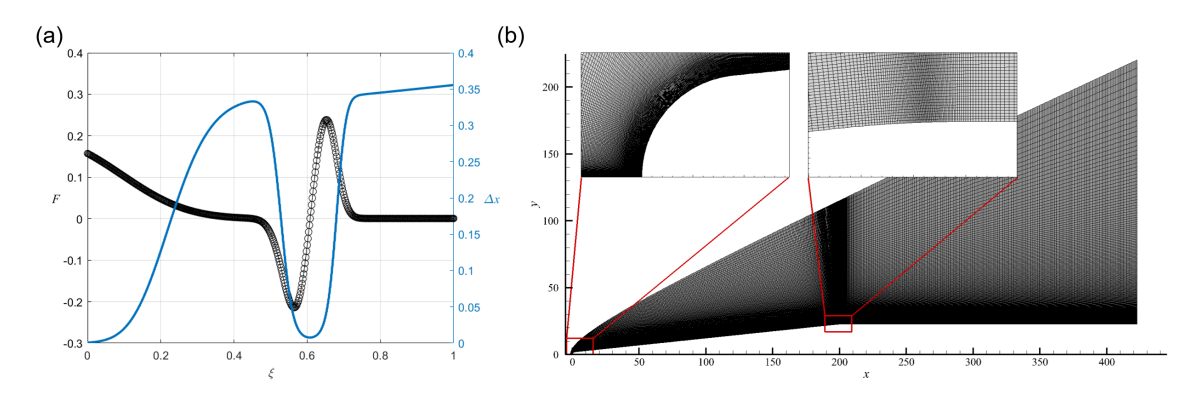


Figure 1 – Computational grid of the swept wing model (a) the distribution of function F and streamwise grid spaces Δx ; (b) grid lines.

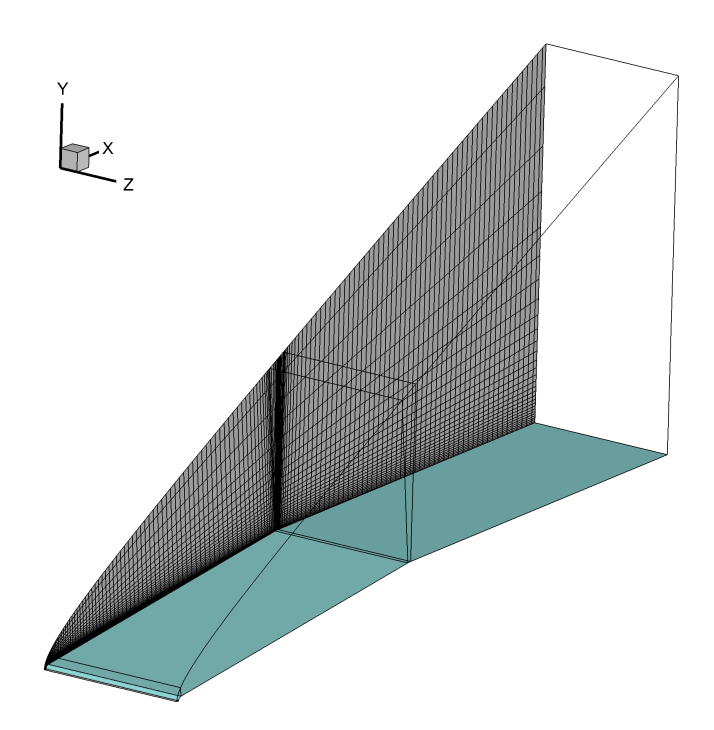


Figure 2 – Three-dimensional sketch of the computational domain of the swept wing model.

3. Results and Discussion

3.1 Baseflow

The results of our basic flow calculations are presented in Fig.3. Our specialized shock-fitting DNS code ensures accurate depiction of the flow patterns. The expansion corner sharply increases the boundary layer thickness, and the effect of expansion waves are clearly seen.

Fig.4 shows the velocity, density, and temperature profiles at typical locations before and after the expansion corner. It can be observed from the figure that the flow parameters conform to the predicted trend of the Prandtl-Meyer theory when passing through the expansion corner, and the change becomes smoother due to the viscous interference brought by the boundary layer. The streamwise velocity gradient parallel to the wall near the wall decreases first and then increases, overall resulting in an increase in velocity. The density decreases significantly overall, and the temperature decreases, with the boundary layer thickness monotonically increasing.

Fig.5 provides the crossflow velocity U_{cf} profile at typical locations before and after the expansion corner, showing that the maximum crossflow velocity first increases and then decreases. The position of the maximum crossflow velocity firstly moves towards the solid surface and then moves away from it. This phenomenom implies a stronger instability near the corner.

Fig.6 presents the $D(\rho DU_{cf})$ distribution of the crossflow velocity profile before and after the ex-

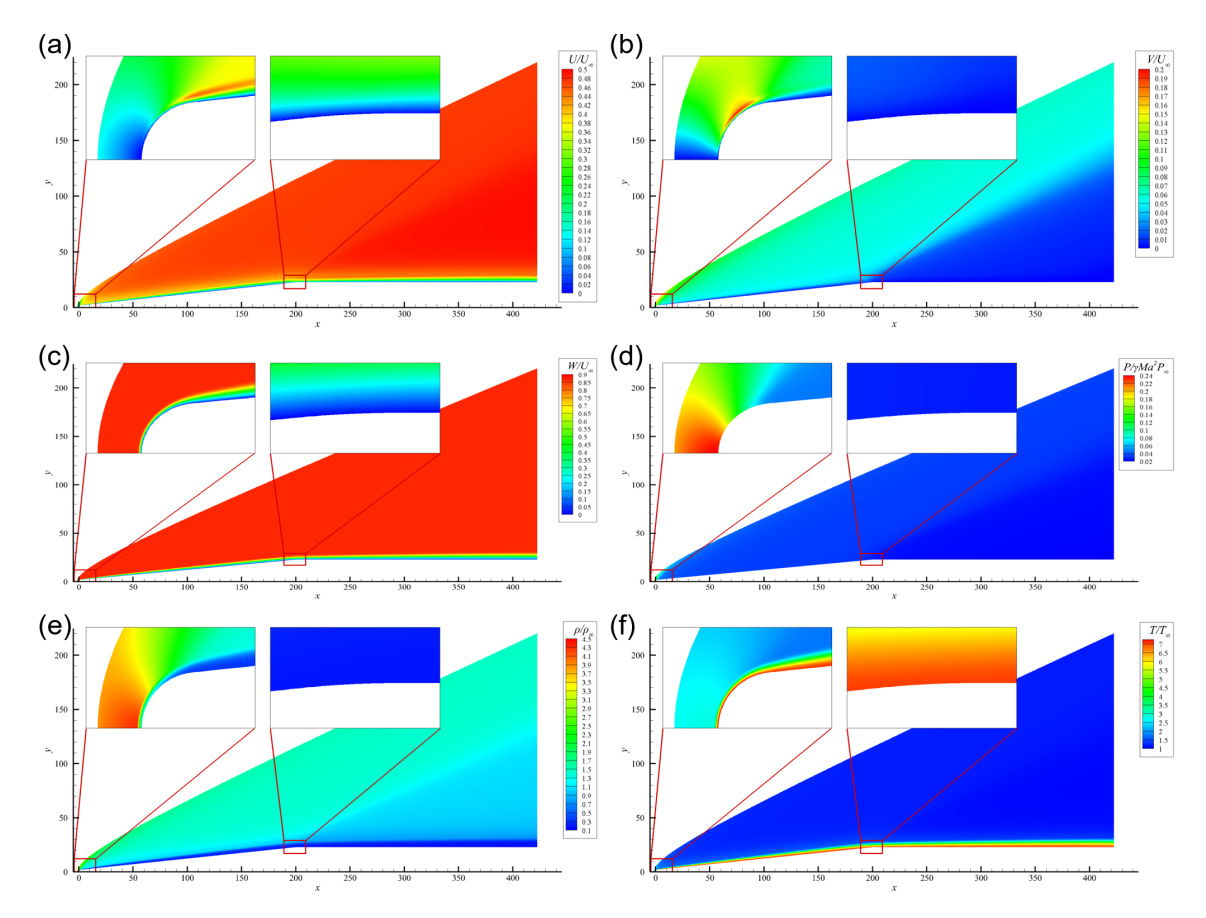


Figure 3 – Contour of dimensionless parameters at Λ=60° (a) U velocity; (b) V velocity; (c) W velocity; (d) pressure; (e) density (f) temperature.

pansion corner at typical locations, where D represents the differential with respect to the normal coordinate. According to the definition of the general inflection point, $D(\rho DU_{cf})=0$, from the curve in the figure, it can be seen that the number of the generalized inflection points stay unchanged, and the wall-normal distance of the inflection point moves awary from the wall. According to inviscid instablility theory, this characteristic usually accompanies increases in growth rates of inviscid unstable modes.

3.2 Stability Characteristics of Stationary Modes

The most unstable mode embodies the typical crossflow mode pattern. Fig.7 shows the pattern of the most unstable perturbation mode at s=89.92, beta=0.797. Fig.7(a) provides the spectrum of the stationary wave. The spectrum consists of both discrete modes and continuous spectrum approximated by discrete points. Under this paper's working condition, there is only one unstable mode in the eigenvalue spectrum. As can be seen from the distribution of its eigenfunctions, the disturbance velocity components in the streamwise direction alternate in opposite peaks along the spanwise direction. Superimposed on the basic flow, this results in a series of streamwise vortical structures, which are characteristic of steady crossflow modes.

After the expansion corner, the crossflow vortices undergo a discernible transformation, assuming a more pronounced inclination and concurrently exhibiting an escalated growth rate, as is shown in Fig.8. The figure presents the comparison of growth rate versus varying spanwise wave numbers at different streamwise positions. As the baseflow advances downstream, the spanwise wave number of the most unstable disturbance wave gradually decreases. The growth rate of the most unstable disturbance mode first decreases gradually with the advancement of the streamwise position and then starts to increase slowly as the basic flow passes through the expansion corner, which may possibly promote transition under this circumstance.

To further investigate the stability characteristics of the flow field, Fig.9 provides the linear stability neutral curve. The abscissa represents the streamwise Reynolds number, and the ordinate repre-

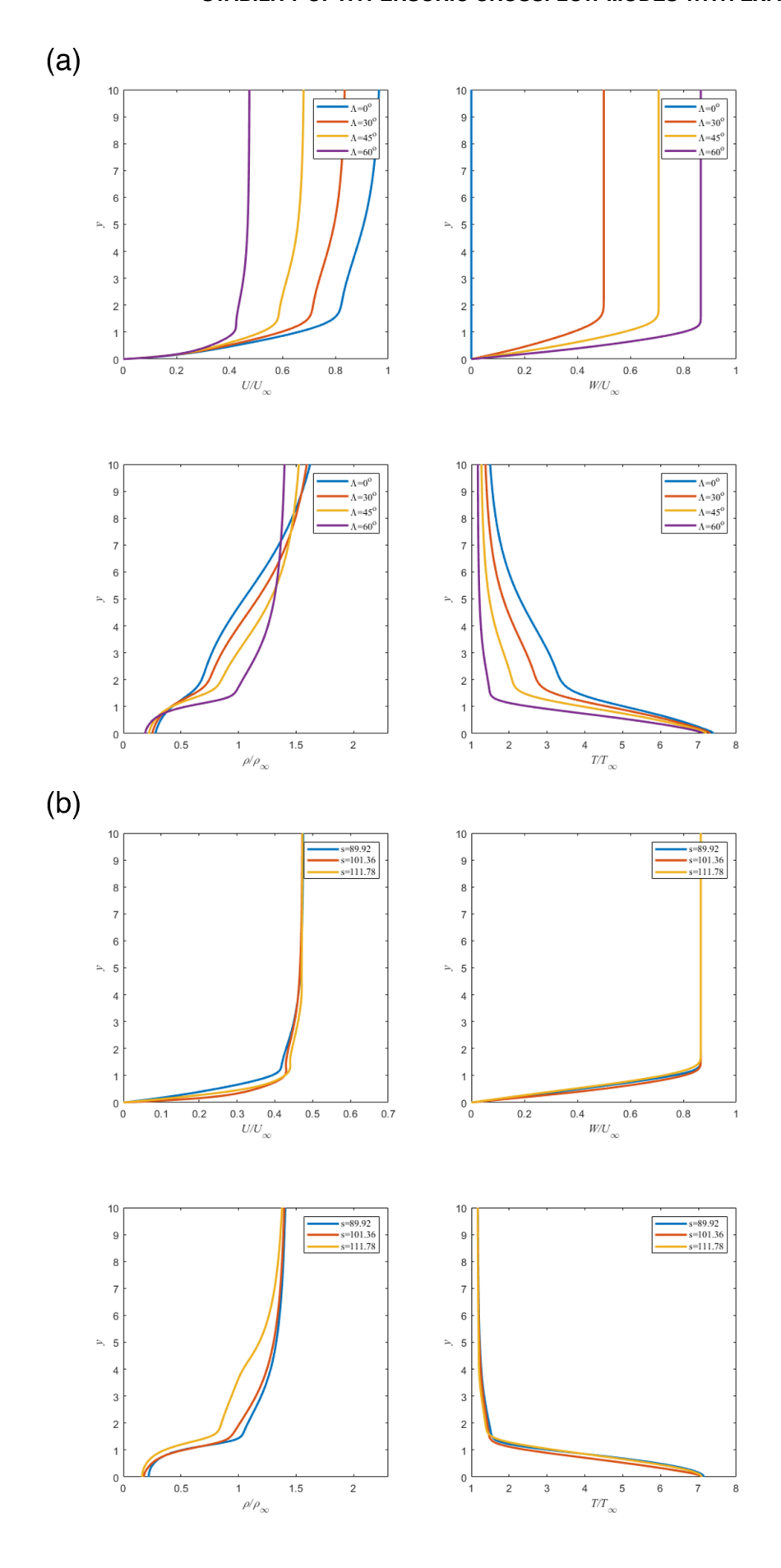


Figure 4 – Profiles of physical parameters for (a) different sweep angles Λ at s=101.36; (b) different streamwise positions at Λ =60°.

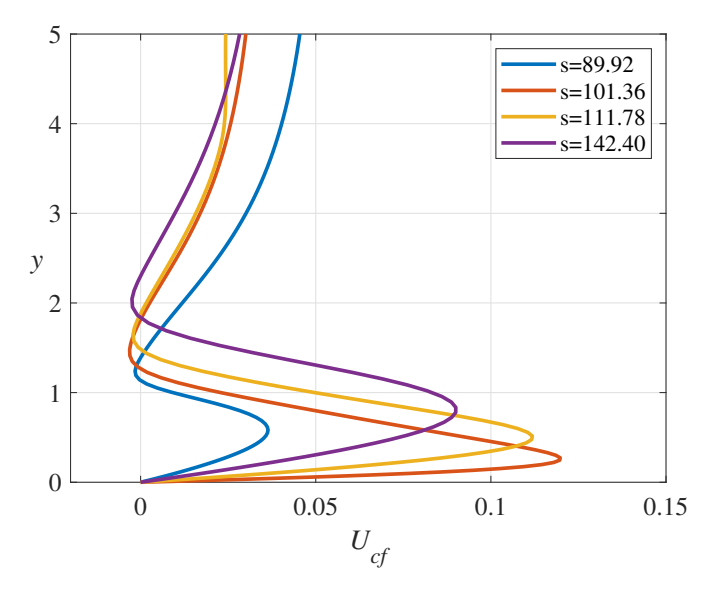


Figure 5 – Profiles of crossflow velocity at different streamwise positions around the expansion corner.

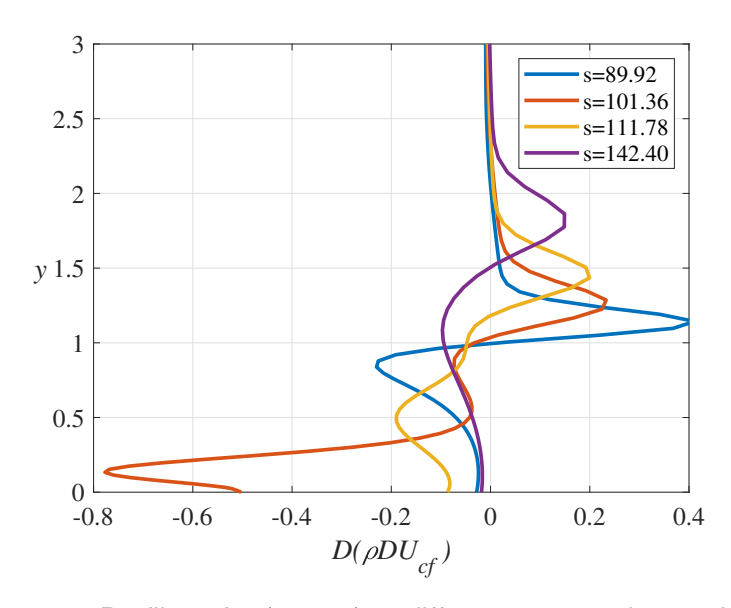


Figure 6 – Profiles of $D(\rho DU_{cf})$ at different streamwise positions.

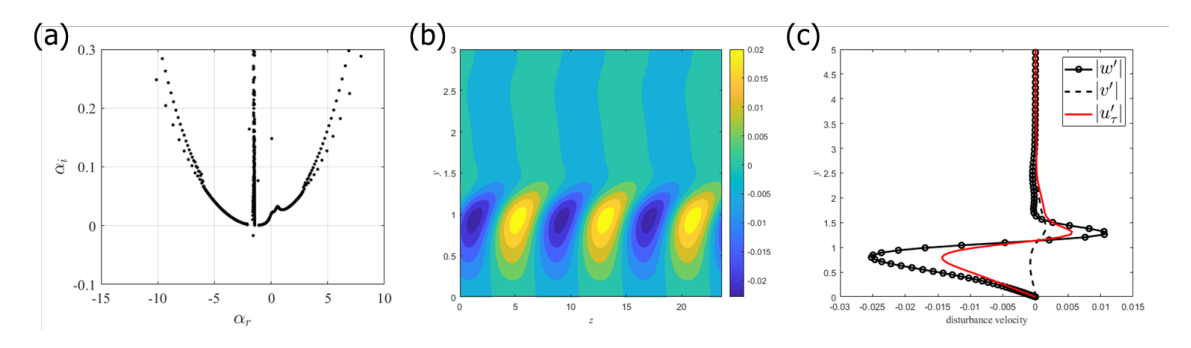


Figure 7 – The most unstable mode at s=89.92 (a) eigenvalue spectrum; (b) contour of streamwise velocity; (c) shape function of perturbation velocity.

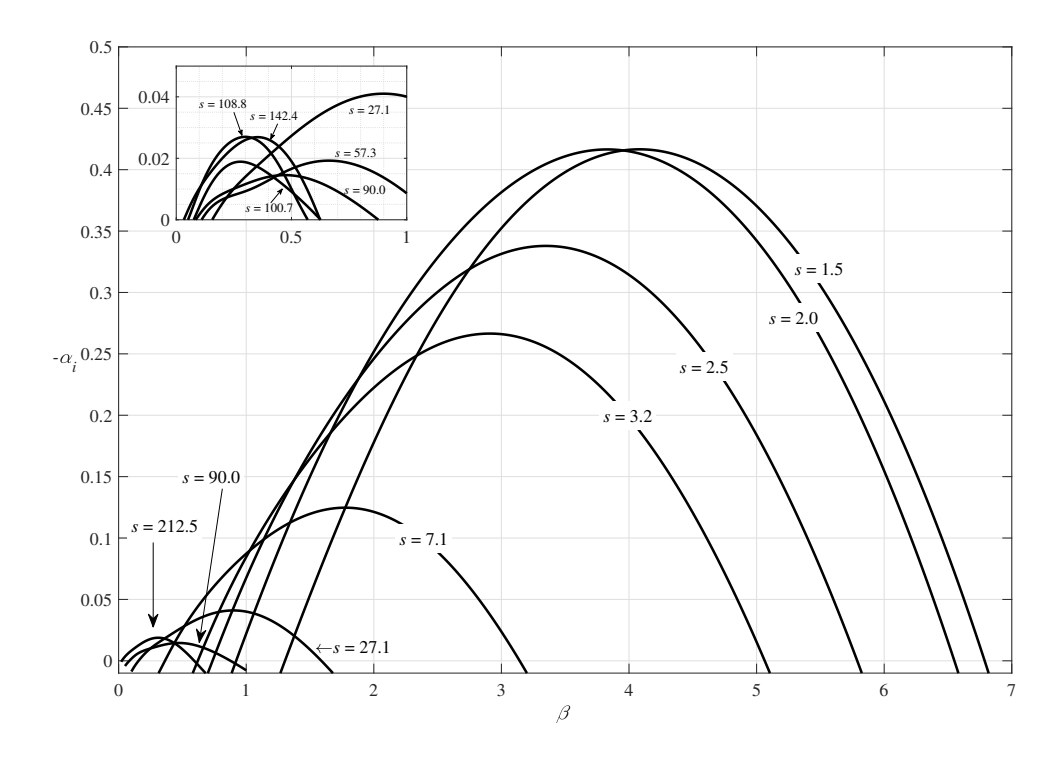


Figure 8 – Growth rate curves at different positions with respect to the spanwise wavenumber.

sents the spanwise wave number. The yellow area represents the stable region where there are no unstable disturbance modes. When the streamwise Reynolds number is approximately 4.3e5, the flow passes through the expansion corner, and a new peak in the growth rate can be observed at this location. This indicates that as the flow advances through the expansion wave, the disturbances within the boundary layer become more unstable. Furthermore, the neutral curves for different sweep angles are presented in Fig.10. As the sweep angle increases from 30 degrees to 60 degrees, the general pattern is consistent, while the maximum growth rate increases significantly as the crossflow becomes stronger.

Further analysis and comparison are conducted on the specific characteristics of the most unstable disturbance waves before and after the expansion corner. Fig.11 presents the shape functions and streamwise velocity contours of the most unstable stationary modes at two typical streamwise positions. These two modes come from the areas near the two peaks of the growth rates shown in Fig.9. Observing the disturbance velocity contour maps of both in Fig.11(b), it can be noticed that their main features are similar, exhibiting the typical characteristics of the crossflow mode. However, from the specific disturbance velocity characteristic functions in Fig.11(a), significant differences can be found between them in terms of sign changes.

Theoretical and experimental studies generally suggest that expansion waves can stabilize flows. Chuvakhov[69] conducted a linear stability analysis of two-dimensional expansion corners and found that in the absence of sweep angle, the second mode dominates. The main effect of the expansion corner on stability characteristics is the increase in boundary layer thickness, which significantly reduced the frequency of the second mode disturbance waves. The growth rates of the high-frequency modes decreased sharply across the corner, while the previously stable low-frequency modes became unstable, leading to a more stable flow phenomenon. In contrast, this study on stationary crossflow modes reaches opposite conclusions. According to Fig.12, on the wedge surface after the blunt head, as the flow progressed in the streamwise direction, the growth rates of the unstable crossflow modes gradually decreased, and the number of general inflection points of the crossflow profile before the expansion wave decreased from three to one. As the flow passed through the expansion wave, the expansion wave caused significant changes in the distribution of flow parameters such as density and temperature, and the number of general inflection points of the crossflow recovered. This

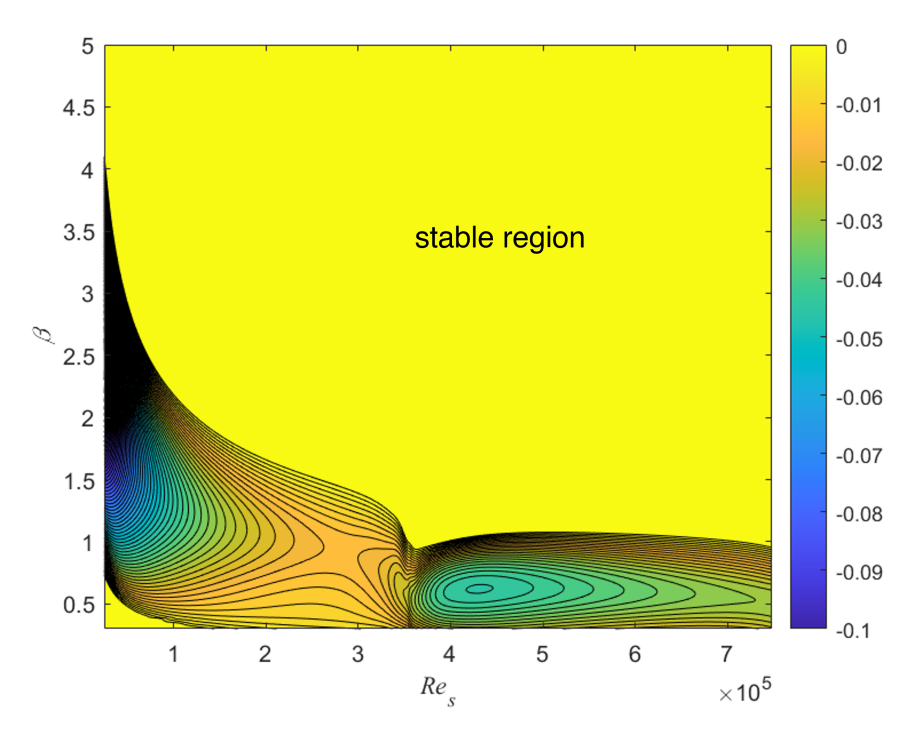


Figure 9 – Neutral curve of the stationary perturbation modes.

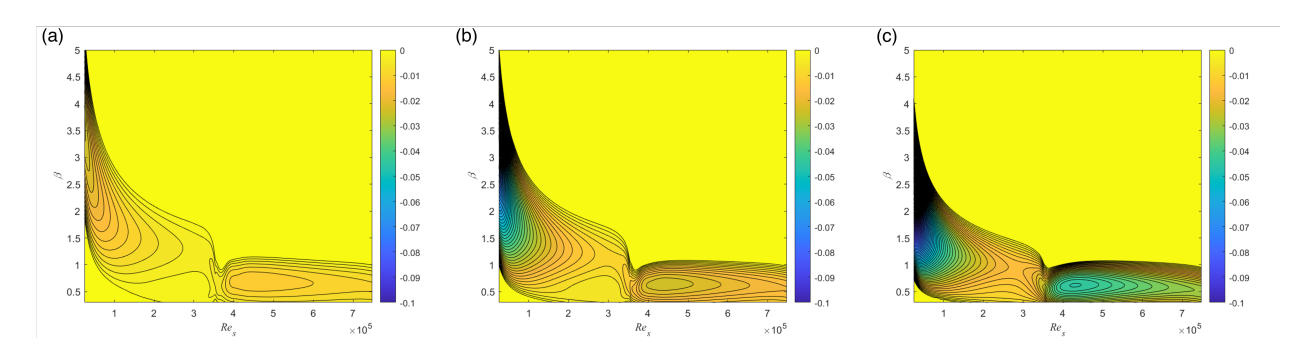


Figure 10 – Neutral curve for different sweep angles (a) $\Lambda = 30^{\circ}$ (b) $\Lambda = 45^{\circ}$ (c) $\Lambda = 60^{\circ}$.

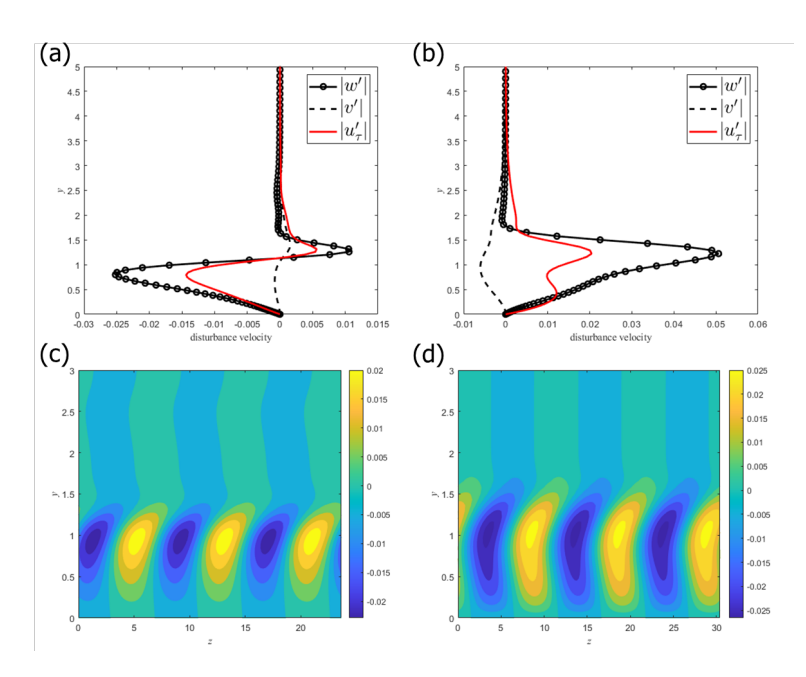


Figure 11 – Comparison of the stationary perturbation modes (a-b) perturbation velocity at s=89.92,121.79; (c-d) streamwise velocity contour at s=89.92,121.79.

stimulation of specific boundary layer steady crossflow modes led to increased instability of the basic flow. In the downstream flat plate stage after the expansion corner, as the boundary layer continued to develop downstream, the growth rate of disturbances decreased again.

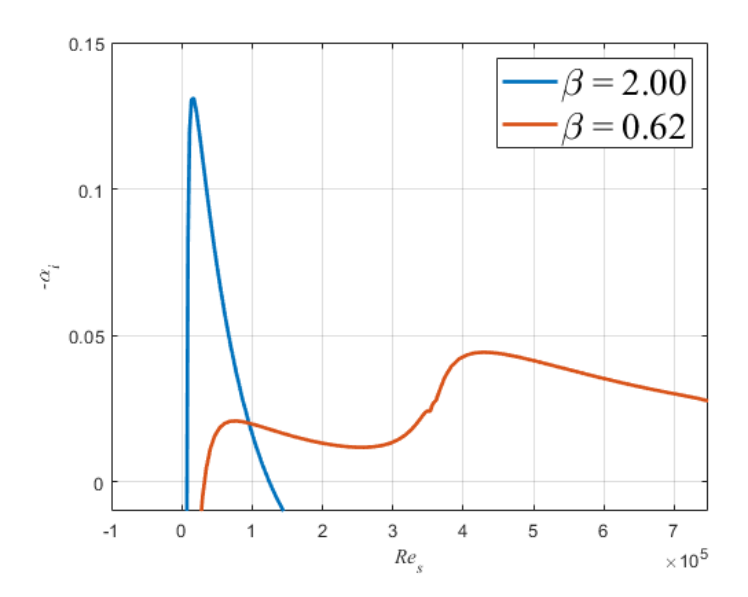


Figure 12 – Growth rate versus streamwise Reynolds number for different spanwise numbers.

4. Conclusion

This work preliminarily investigates the effect of expansion corner on the linear stability of the swept wing hypersonic boundary-layer flow. The high-accuracy baseflow of a swept wing with an expansion corner is calculated using the finite difference shock-fitting method. Based on this, linear stability tools are employed to explore the influence of the expansion corner on the linear instability characteristics of the stationary crossflow modes in the hypersonic boundary layer.

The shock-fitting method provides accurate and smooth baseflow. At the expansion corner, the position of general inflection points of the crossflow velocity moves away from the solid surface, which affects the inviscid instability characteristics of the boundary layer.

Under the working condition of this paper, the most unstable stationary disturbance mode in the swept wing boundary layer before and after the expansion corner is the crossflow mode. There is a significant change in the disturbance velocity characteristics of the stationary crossflow mode before and after the expansion corner.

The stationary crossflow mode before the expansion corner gradually decays in growth rate as it develops in the streamwise direction. The appearance of the expansion wave makes the stationary crossflow mode more unstable, and after passing through the expansion corner, the flow stabilizes again as it develops in the streamwise direction. The result indicates that the existence of the expansion corner may greatly destabilize the laminar base flow and thus promote transition.

In the future, we will continue investigating the non-linear behaviour of unstable modes which have been identified in this study. We plan to employ secondary instability theory (SIT) to monitor the change of secondary modes in the neighbourhood of the expansion corner. Furthermore, we would conduct a DNS study to compare the results with SIT.

5. Contact Author Email Address

Mail to: fs-dem@tsinghua.edu.cn

6. Copyright Statement

The authors confirm that they, and/or their company or organization, hold copyright on all of the original material included in this paper. The authors also confirm that they have obtained permission, from the copyright holder of any third party material included in this paper, to publish it as part of their paper. The authors confirm that

they give permission, or have obtained permission from the copyright holder of this paper, for the publication and distribution of this paper as part of the ICAS proceedings or as individual off-prints from the proceedings.

7. Acknowledgements

Support from the National Key Research and Development Plan of China through project No. 2019YFA0405200, the National Key Project (Grant No. GJXM92579), NSFC grant 12202242 and 12172195, Project No. 1912, Yancheng MetaStone Co. is gratefully acknowledged.

References

- [1] Mack L M. Boundary-layer linear stability theory. Agard rep, 709(3), pp 1-3, 1984.
- [2] Reed H L and Saric W S. Stability of three-dimensional boundary layers. *Annual Review of Fluid Mechanics*, 21(1), pp 235–284, 1989.
- [3] Hall P. The Görtler vortex instability mechanism in three-dimensional boundary layers. *Proceedings of the Royal Society of London. A. Mathematical and Physical Sciences*, Vol. 399, No. 1816, pp 135-152, 1985.
- [4] Craig S A and Saric W S. Crossflow instability in a hypersonic boundary layer. *Journal of Fluid Mechanics*, Vol. 808, pp 224-244, 2016.
- [5] Deyhle H and Bippes H. Disturbance growth in an unstable three-dimensional boundary layer and its dependence on environmental conditions. *Journal of Fluid Mechanics*, Vol. 316, pp 73-113, 1996.
- [6] Gray W E, The effect of wing sweep on laminar flow, Rae Tm Aero, Vol. 227, pp 1952, 1952.
- [7] Owen P R and Randall D G. Boundary layer transition on a sweptback wing. *Royal Aircraft Establishment*, 1952.
- [8] Squire H B. Addendum on sweepback and transition. Rae Tm Aero, Vol. 277, 1952.
- [9] Stuart J T. An Interim Note on the Stability of the Boundary-layer on a Swept Wing. ARC, 1952.
- [10] Smith N H. Exploratory investigation of laminar-boundary-layer oscillations on a rotating disk, 1947.
- [11] Gregory N, Stuart J T and Walker W S. On the stability of three-dimensional boundary layers with application to the flow due to a rotating disk, *Philosophical Transactions of the Royal Society of London. Series A, Mathematical and Physical Sciences*, Vol. 248, No. 943, pp 155–199, 1955.
- [12] Brown W B. Numerical calculation of the stability of crossflow profiles in laminar boundary layers on a rotating disc and on a swept wing and an exact calculation of the stability of the Blasius Velocity Profile. Northrop Rep. NAI-59-5 (BLC-117), 1959.
- [13] Brown W B. A stability criterion for three-dimensional laminar boundary layers. *Boundary layer and flow control*, Elsevier, pp. 913–923, 1961.
- [14] Cebeci T and Stewartson K. On Stability and Transition in Three-Dimensional Flows. *AIAA Journal*, Vol. 18, No. 4, pp. 398–405, Apr. 1980.
- [15] Wilkinson S and Malik M. Stability experiments in rotating-disk flow. *16th Fluid and Plasmadynamics Conference*, paper 1760, 1983.
- [16] Malik M R, Wilkinson S P, and Orszag S A. Instability and transition in rotating disk flow. *AIAA Journal*, Vol. 19, No. 9, pp. 1131–1138, Sep. 1981, doi: 10.2514/3.7849.
- [17] Kobayashi R, Kohama Y, and Takamadate Ch. Spiral vortices in boundary layer transition regime on a rotating disk. *Acta Mechanica*, Vol. 35, No. 1–2, pp. 71–82, Mar. 1980, doi: 10.1007/BF01190058.
- [18] Mack L. The wave pattern produced by a point source on a rotating disk. *23rd Aerospace Sciences Meeting*, Reno, NV, U.S.A.: American Institute of Aeronautics and Astronautics, Jan. 1985, doi: 10.2514/6.1985-490.
- [19] Malik M R. The neutral curve for stationary disturbances in rotating-disk flow. *Journal of Fluid Mechanics*, Vol. 164, pp. 275–287, 1986.
- [20] Fedorov B I, Plavnik G Z, Prokhorov I V, and Zhukhovitskii L G. Transitional flow conditions on a rotating disk. *Journal of Engineering Physics*, Vol. 31, pp. 1448–1453, 1976.
- [21] Faller A J. Instability and transition of disturbed flow over a rotating disk. *Journal of Fluid Mechanics*, Vol. 230, pp. 245–269, 1991.
- [22] Malik M R and Spall R E. On the stability of compressible flow past axisymmetric bodies. *Journal of Fluid Mechanics*, Vol. 228, pp. 443–463, 1991.
- [23] Hall P. An asymptotic investigation of the stationary modes of instability of the boundary layer on a rotating disc. *Proceedings of the Royal Society of London. A. Mathematical and Physical Sciences*, Vol. 406, No. 1830, pp. 93–106, 1986.

- [24] Morkovin M V. Understanding transition to turbulence in shear layers. Defence Technical Information Center, USA, 1983.
- [25] Bacon J W, Tucker V L, and Pfenninger W. Experiments on a 30" Sept 12 Percent Thick Symmetrical Laminar Suction Wing in the 5-ft. by 7-ft. University of Michigan Tunnel. Northrop Corporation, Norvair Division Report NOR-59-328 (BLC-119), 1959.
- [26] Gault D E. An Experimental Investigation of Boundary-Layer Control for Drag Reduction of a Swept-Wing Section at Low Speed and High Reynolds Numbers. National Aeronautics and Space Administration, 1960.
- [27] Pfenninger W and Bacon J W Jr. About the development of swept laminar suction wings with full chord laminar flow. *Boundary Layer and Flow Control*, Elsevier, pp. 1007–1032, 1961.
- [28] Mack L. On the stability of the boundary layer on a transonic swept wing. In *17th Aerospace Sciences Meeting*, 1979, p. 264.
- [29] El-Hady N. On the stability of three-dimensional compressible nonparallel boundary layers. In *13th Fluid* and *PlasmaDynamics Conference*, American Institute of Aeronautics and Astronautics, 1980.
- [30] Mack L M. Compressible Boundary-Layer Stability Calculations for Sweptback Wings with Suction. *AIAA Journal*, Vol. 20, No. 3, pp. 363–369, Mar. 1982.
- [31] Nayfeh A H and Padhye A. Relation between Temporal and Spatial Stability in Three-Dimensional Flows. *AIAA Journal*, Vol. 17, No. 10, pp. 1084–1090, Oct. 1979.
- [32] Nayfeh A H. Stability of three-dimensional boundary layers. *AIAA Journal*, Vol. 18, No. 4, pp. 406–416, 1980.
- [33] Padhye A and Nayfeh A. Nonparallel stability of three-dimensional flows. In *14th Fluid and Plasma Dynamics Conference*, Palo Alto, CA, U.S.A.: American Institute of Aeronautics and Astronautics, Jun. 1981.
- [34] Gaster M. A note on the relation between temporally-increasing and spatially-increasing disturbances in hydrodynamic stability. *Journal of Fluid Mechanics*, Vol. 14, No. 2, pp. 222–224, 1962.
- [35] Müller B and Bippes H. Experimental study of instability modes in a three-dimensional boundary layer. In *AGARD*, 1989.
- [36] Bippes H and Nitschke-Kowsky P. Experimental study of instability modes in a three-dimensional boundary layer. AIAA Journal, Vol. 28, No. 10, pp. 1758–1763, 1990.
- [37] Bippes H. Basic experiments on transition in three-dimensional boundary layers dominated by crossflow instability. *Progress in Aerospace Sciences*, Vol. 35, No. 4, pp. 363–412, 1999.
- [38] Dagenhart J, Stack J, Saric W, and Mousseux M. Crossflow-vortex instability and transition on a 45 deg swept wing. In *20th Fluid Dynamics, Plasma Dynamics and Lasers Conference*, 1989, p. 1892.
- [39] Kohama Y, Saric W S, and Hoos J A. A high-frequency, secondary instability of crossflow vortices that leads to transition. Presented at the In: Boundary layer transition and control; Proceedings of the Conference, Univ. of Cambridge, United Kingdom, Apr. 8-12, 1991 (A93-17251 04-34), Royal Aeronautical Society, 1991.
- [40] Saric W S, Reed H L, and White E B. Stability and transition of three-dimensional boundary layers. *Annual Review of Fluid Mechanics*, Vol. 35, No. 1, pp. 413–440, 2003.
- [41] Arnal D and Juillen J. Three-dimensional transition studies at ONERA/CERT. In 19th AIAA, Fluid Dynamics, Plasma Dynamics, and Lasers Conference, 1987, p. 1335.
- [42] Malik M R, Li F, Choudhari M M, and Chang C-L. Secondary instability of crossflow vortices and sweptwing boundary-layer transition. *Journal of Fluid Mechanics*, Vol. 399, pp. 85–115, 1999.
- [43] Haynes T S and Reed H L. Simulation of swept-wing vortices using nonlinear parabolized stability equations. *Journal of Fluid Mechanics*, Vol. 405, pp. 325–349, 2000.
- [44] Janke E and Balakumar P. On the secondary instability of three-dimensional boundary layers. *Theoretical and Computational Fluid Dynamics*, Vol. 14, No. 3, pp. 167–194, 2000.
- [45] Koch W, Bertolotti F P, Stolte A, and Hein S. Nonlinear equilibrium solutions in a three-dimensional boundary layer and their secondary instability. *Journal of Fluid Mechanics*, Vol. 406, pp. 131–174, 2000.
- [46] Theofilis V. Global Linear Instability. *Annual Review of Fluid Mechanics*, Vol. 43, No. 1, pp. 319–352, 2011, doi: 10.1146/annurev-fluid-122109-160705.
- [47] Högberg M and Henningson D. Secondary instability of cross-flow vortices in Falkner–Skan–Cooke boundary layers. *Journal of Fluid Mechanics*, Vol. 368, pp. 339–357, 1998.
- [48] Wassermann P and Kloker M. Transition mechanisms induced by travelling crossflow vortices in a three-dimensional boundary layer. *Journal of Fluid Mechanics*, Vol. 483, pp. 67–89, 2003, doi: 10.1017/S0022112003003884.
- [49] Balachandar S, Streett C L, and Malik M R. Secondary instability in rotating-disk flow. Journal of Fluid

- Mechanics, Vol. 242, pp. 323-347, 1992.
- [50] Kohama Y. Study on boundary layer transition of a rotating disk. *Acta Mechanica*, Vol. 50, No. 3, pp. 193–199, 1984.
- [51] Fischer T M and Dallmann U. Primary and secondary stability analysis of a three-dimensional boundary-layer flow. *Physics of Fluids A: Fluid Dynamics*, Vol. 3, No. 10, pp. 2378–2391, 1991.
- [52] Meyer F and Kleiser L. Numerical investigation of transition in 3D boundary layers. In *Fluid Dynamics of Three-Dimensional Turbulent Shear Flows and Transition*, pp. 16–1, 1989.
- [53] Malik M R, Li F, and Chang C-L. Nonlinear crossflow disturbances and secondary instabilities in sweptwing boundary layers. In *IUTAM Symposium on Nonlinear Instability and Transition in Three-Dimensional Boundary Layers*, Springer, 1996, pp. 257–266.
- [54] Parziale N J, Shepherd J E, and Hornung H G. Observations of hypervelocity boundary-layer instability. *Journal of Fluid Mechanics*, Vol. 781, pp. 87–112, 2015.
- [55] Schmisseur J, Young J, and Schneider S. Measurements of boundary-layer transition on the flat sidewall of a rectangular Mach 4 quiet-flow nozzle. In *34th Aerospace Sciences Meeting and Exhibit*, 1996, p. 852.
- [56] Dolvin D. Hypersonic international flight research and experimentation (HIFiRE) fundamental science and technology development strategy. In 15th AIAA International Space Planes and Hypersonic Systems and Technologies Conference, 2008, p. 2581.
- [57] Kimmel R L et al. First and fifth hypersonic international flight research experimentation's flight and ground tests. *Journal of Spacecraft and Rockets*, Vol. 56, No. 2, pp. 421–431, 2019.
- [58] Ward C, Henderson R, and Schneider S P. Secondary instability of stationary crossflow vortices on an inclined cone at Mach 6. In *45th AIAA Fluid Dynamics Conference*, 2015, p. 2773.
- [59] Kocian T S et al. Hypersonic crossflow instability. *Journal of Spacecraft and Rockets*, Vol. 56, No. 2, pp. 432–446, 2019.
- [60] Li F, Choudhari M, Paredes P, and Duan L. High-frequency instabilities of stationary crossflow vortices in a hypersonic boundary layer. *Physical Review Fluids*, Vol. 1, No. 5, p. 053603, 2016.
- [61] Chen X, Dong S, Tu G, Yuan X, and Chen J. Boundary layer transition and linear modal instabilities of hypersonic flow over a lifting body. *Journal of Fluid Mechanics*, Vol. 938, p. A8, 2022.
- [62] Xu G, Chen J, Liu G, Dong S, and Fu S. The secondary instabilities of stationary cross-flow vortices in a Mach 6 swept wing flow. *Journal of Fluid Mechanics*, Vol. 873, pp. 914–941, 2019, doi: 10.1017/jfm.2019.397.
- [63] Chen J, Dong S, Chen X, Yuan X, and Xu G. Stationary cross-flow breakdown in a high-speed swept-wing boundary layer. *Physics of Fluids*, Vol. 33, No. 2, 2021.
- [64] Xi Y, Ren J, Wang L, and Fu S. Receptivity and stability of hypersonic leading-edge sweep flows around a blunt body. *Journal of Fluid Mechanics*, Vol. 916, p. R2, 2021, doi: 10.1017/jfm.2021.217.
- [65] Chen X, Xi Y, Ren J, and Fu S. Cross-flow vortices and their secondary instabilities in hypersonic and highenthalpy boundary layers. *Journal of Fluid Mechanics*, Vol. 947, p. A25, 2022, doi: 10.1017/jfm.2022.607.
- [66] Ren J and Fu S. Secondary instabilities of Görtler vortices in high-speed boundary layer flows. *Journal of Fluid Mechanics*, Vol. 781, pp. 388–421, 2015.
- [67] Xi Y, Ren J, and Fu S. Hypersonic attachment-line instabilities with large sweep Mach numbers. *Journal of Fluid Mechanics*, Vol. 915, p. A44, 2021.
- [68] Zhong X. High-order finite-difference schemes for numerical simulation of hypersonic boundary-layer transition. *Journal of Computational Physics*, Vol. 144, No. 2, pp. 662-709, 1998.
- [69] Chuvakhov P V, Egorov I V, Ilyukhin I M, Obraz A O, and Fedorov A V. Boundary-layer instabilities in supersonic expansion corner flows. *AIAA Journal*, Vol. 59, No. 9, pp. 3398-3405, 2021.